Large eddy simulation of a forced round turbulent buoyant plume in neutral surroundings

By A. J. Basu AND N. N. Mansour

1. Motivation and objectives

Buoyant flows play an important role in various technological and environmental issues. For example, dispersal of pollutants, smoke, or volcano exhaust in the atmosphere, vertical motion of air, formation of clouds and other weather systems, and flows in cooling towers and fires are all determined primarily by buoyancy effects. The buoyancy force in such flows can originate from either a heat source or due to different densities between a fluid and its surroundings. Whatever the cause, the flow can be understood by studying the effects of the tight coupling between the thermal and the velocity fields since density differences can be characterized as temperature differences.

Heat addition to turbulent flows always leads to very complicated behavior, greatly affecting their structure and entrainment characteristics. Heat can be added in many different ways into a flow; for example: at the source, or off-source. These two methods of heat addition can have very different effects on the development of the flow. Basu & Narasimha (1999) studied the effects of off-source volumetric heating (similar to that due to latent heat release in a cloud, for example) using Direct Numerical Simulation (DNS) of a circular jet-like flow and found that the large-scale structures break down and entrainment is inhibited. Here we look at a round turbulent plume with both momentum and buoyancy added at the source, using the tools of Large Eddy Simulation (LES).

Similarity solutions of turbulent circular plumes have been proposed in the past by Zeldovich (1937) and Batchelor (1954) based on the Boussinesq hypothesis, which assumes that the density changes in the flow are small compared to the ambient density, an assumption that is valid in regions away from the plume source. In a neutral environment (no change in ambient density with height), the mean vertical velocity and buoyancy acceleration are given respectively by:

$$W = F_o^{1/3} z^{-1/3} A_W e^{-B_W \eta^2}, \tag{1}$$

$$g\frac{\Delta\rho}{\rho_a} = F_o^{2/3} z^{-5/3} A_T e^{-B_T \eta^2}, \tag{2}$$

where W is the mean vertical velocity along the axis of the plume, F_o is the rate of addition of buoyancy, z is the height (from the buoyancy source), g is acceleration due to gravity, $\Delta\rho$ is the density difference at a point with respect to the ambient density ρ_a, and A_W, B_W are the parameters which quantify the Gaussian fit to the mean velocity profile, while A_T, B_T are the corresponding ones for the density (or, equivalently, temperature) profile; η represents the similarity variable

$\eta = r/z$, where r is the radial distance at any z. For a flow involving sources of both momentum and buoyancy such as the one studied here, it is known that the buoyancy effects overwhelm the momentum added at the source, typically after an axial distance $z/L_M > 5$, where

$$L_M = M_o^{3/4}/F_o^{1/2} \tag{3}$$

is the so-called Morton lengthscale. The source momentum flux M_o and buoyancy flux F_o are defined as:

$$M_o = 2\pi \int_0^{R_o} W^2 r dr, \tag{4}$$

$$F_o = 2\pi \int_0^{R_o} W g \frac{\Delta\rho}{\rho_a} r dr, \tag{5}$$

where R_o is the source radius.

The forced buoyant plume has been the object of many experimental investigations in the past (see List 1982, Rodi 1986 for reviews). Most notable among the reported experiments are the ones by Rouse *et al.* (1952), Nakagome & Hirata (1977), Papanicolaou & List (1988), and Shabbir & George (1994) in that they report widely different results. The primary disagreements among the various experimental results are regarding the centerline values of mean velocity and buoyancy profiles as well as the plume spreading rate. For example, the spread of reported experimental values (as compiled in Shabbir & George) are given here inside brackets for the different parameters for Gaussian fit of profiles described above: $A_W = (3.4 - 4.7), B_W = (55 - 96), A_T = (9.1 - 14.28), B_T = (48 - 71)$. Clearly the scatter is quite large.

The discrepancies between different experimental data are likely to be due to various factors, some of which are detailed below: (i) boundary effects of the solid wall lateral boundaries and presence of reverse or co-flow can influence the entrainment, (ii) measurements may not have been carried out in fully developed turbulent region in some cases, (iii) hot-wire anemometer measurements are known to be insensitive to direction, and therefore the measurements made outside the half-width of the plume may not be reliable in such cases. Since F_o is used to scale for self-similarity, a lot crucially depends on the accurate determination of F_o, the measurement of which, unfortunately, can be influenced by the experimental errors. As will be seen later, the above mentioned problems with the available experimental data somewhat constrain the validation of numerical predictions made in this study.

2. Accomplishments

2.1 Governing equations

In the present study, we aim to compute the evolution of a circular plume in neutral surroundings with momentum and buoyancy added only at the source. Since the density differences away from the source of a plume are known to be small compared to ambient density, the Boussinesq approximation is assumed to be valid.

whereby the effects of density variations are modeled by a source term in the momentum equations. The resulting equations in the non-dimensional form are given by:

$$\nabla \cdot \mathbf{u} = 0, \tag{6}$$

$$\frac{\partial \mathbf{u}}{\partial t} + \nabla \cdot (\mathbf{uu}) = -\nabla p + \frac{1}{Re}\nabla^2 \mathbf{u} + \frac{Gr}{Re^2}\Theta \hat{z}, \tag{7}$$

$$\frac{\partial \Theta}{\partial t} + (\mathbf{u} \cdot \nabla)\Theta = \frac{1}{RePr}\nabla^2 \Theta, \tag{8}$$

where $\mathbf{u}$ is the velocity vector, p is pressure, $\Theta = (T - T_a)/(T_o - T_a)$ is the temperature difference (where T, T_a, T_o are the absolute temperatures, respectively at a given point, the ambient and the plume source). The non-dimensional governing parameters are:

$Re = U_o D_o/\nu$ = Reynolds number,

$Pr = \nu/\kappa$ = Prandtl number,

$Gr = \alpha g(T_o - T_a)D_o^3/\nu^2$ = Grashoff number,

where U_o and D_o are respectively the velocity at and diameter of the source, ν is the kinematic viscosity of the fluid, κ the thermal diffusivity, α the coefficient of thermal expansion, and g the acceleration due to gravity. The last term in the momentum equation (7) above is the buoyancy source term and acts only along the vertical z direction.

2.2 Numerical technique

Following the standard approach for LES, the above equations are passed through a spatial filter, and the resulting effects of the subgrid scales are modeled. In the present study, we have used the well-known dynamic model for this purpose (Germano *et al.* 1990, Lilly 1992).

The spherical polar coordinate system (r, θ, ϕ, along the radial vector, lateral, and azimuthal directions respectively) is used here since, for the present flow with its conical mean growth, a spherical system allows for a well-balanced resolution of the flow field with a reasonable number of grid points. The present computer code is a modified version of that developed by Boersma *et al.* (1998) for cold jets. The basic numerical formulation being similar, the reader is referred to the above-mentioned paper for various implementation details. We will only describe some fundamental features of the numerical scheme and also the extensions made in the present study.

Second order accurate finite volume technique is used to approximate the equations of motion in space, along with a second order explicit Adams-Bashforth scheme for time-integration. Pressure correction technique is employed after each Adams-Bashforth step in order to ensure that the velocity field remains divergence-free at all times. The resultant Poisson equation is solved using fast Fourier transform along the periodic (ϕ) direction and cyclic reduction along the other two directions. The convective term in the temperature equation is treated using a TVD scheme (see, e.g., Vreugdenhill & Koren 1993) in order to keep Θ between the bounds 0 and 1.

2.3 Boundary conditions

The flow considered, as mentioned earlier, is a forced circular buoyant plume issuing from an orifice in a wall at the bottom end of the computational domain; we assume a tophat velocity profile. The boundary conditions at the inflow are therefore:

$u_r = W_o cos\theta$ in the orifice and $u_r = 0$ elsewhere,

$u_\theta = -W_o sin\theta$ in the orifice and $u_\theta = 0$ elsewhere,

$u_\phi = 0$,

$\Theta = 1$ in the orifice and $\Theta = 0$ elsewhere,

where $W_o = 1$ is the non-dimensional axial velocity in the orifice (diameter $D_o = 1$). Note that u_r, u_θ, u_ϕ here represent velocity components along the r, θ, ϕ directions respectively.

At the lateral boundary, the so-called traction-free boundary conditions are used (Gresho 1991):

$$\sigma_{ij} \cdot n_j = 0, \tag{9}$$

where σ_{ij} is the stress tensor, and n_j the unit normal to the boundary. The advantage of this boundary condition is that entrainment is allowed (Boersma *et al.* 1998). For temperature, the normal derivative is set to zero at the lateral boundary:

$$\frac{\partial \Theta}{\partial n} = 0. \tag{10}$$

At the outflow boundary, we use the so-called advective boundary condition, as in Boersma *et al.* . Thus, for any velocity component u, we have

$$\frac{\partial u}{\partial t} = -W_A \frac{\partial u}{\partial r}, \tag{11}$$

where the advective velocity W_A is a function of θ and is obtained at each step by averaging the streamwise velocity along ϕ near the outflow domain and setting negative values of W_A to zero. As mentioned in Boersma *et al.* , this outflow boundary condition is not entirely satisfactory for the present flow. Therefore, we also add a so-called "buffer zone" near the outflow region where terms similar to $-\lambda(\mathbf{u} - \mathbf{u}_{target})$ are added to the momentum equation in order to damp the turbulence in this region; here λ is a space-varying positive parameter ($\lambda = 1$ at the outflow boundary and decays to 0 outside the buffer zone), and $\mathbf{u}_{target}$ is a desired velocity field. Typically, an analytically or experimentally derived mean velocity field near the outflow domain is used as $\mathbf{u}_{target}$.

2.4 Results

The parameters defining the flow in the present computation are chosen so as to closely correspond to the experimental situation for the round turbulent buoyant plume reported in Shabbir & George (1994). Therefore, we use the following non-dimensional numbers that completely determine the flow: $Re = 3500, Pr = 0.7, Gr = 8.575 \times 10^6$. White noise with a peak amplitude of 0.02 has been added at

all times at the source in order to mimic the disturbances in the exit profile reported in the experiment.

The computations are carried out in a domain that extends to 50 diameters downstream of the source. The domain encompasses a conical volume of lateral angle $\pi/15$, with a virtual origin that is 15 diameters upstream of the orifice. This volume is discretized using a grid of size ($N_r = 128, N_\theta = 40, N_\phi = 32$), where N_r, N_θ, N_ϕ are the number of finite-volume cells along the (r, θ, ϕ) directions respectively. The grid spacing along r increases linearly from 0.1122 near the source to 0.669 near the outflow boundary. Grid spacing is constant along θ and ϕ.

The computations are carried on for 70,000 time-steps in the present study. The time taken on a 8-processor SGI Origin 2000 is of the order of 1 second per step.

In the results presented below, the data from the last 10 diameters are not shown since the effects of outflow boundary conditions and buffer zone are likely to be significant there.

2.4.1 Temperature distribution

The distribution of non-dimensional temperature difference Θ in a buoyant plume is an important parameter since it represents the driving force behind the flow, especially after a few diameters downstream of the orifice where the effect of initial momentum becomes insignificant in comparison with the buoyancy force. In Fig. 1(a), we present a contour plot of the typical instantaneous distribution of Θ over a vertical section passing through the axis of the plume. The contour levels go from 0.1 to 1 in steps of 0.1. Very clearly, high values of Θ are limited to the region close to the orifice. Temperature differences higher than 0.2 (the non-dimensionalized temperature difference at the source being $\Theta = 1$) exist only within the first 10 diameters or so. After about 20 diameters from the source, peak Θ anywhere in the plume has fallen to 0.1 or below, indicating that the Boussinesq approximation is valid over the self-similar region of the flow, the region of our primary interest.

The lower levels of Θ (those between 0.01 and 0.1) at the same time are highlighted in Fig. 1(b) in order to complete this instantaneous picture of temperature distribution. The important point to note is that there does not appear to be any "holes" in the temperature distribution, unlike those reported for passive scalar (Papantoniou & List 1989). Visual analysis of data indicated similar qualitative nature of distribution at other times.

2.4.2 Streamwise variation of momentum and buoyancy fluxes

The similarity solution for plumes (e.g., Batchelor 1954) suggests that, for an ideal gas plume in a neutral environment, the buoyancy flux is conserved. The momentum flux, in comparison, grows with streamwise distance due to entrainment. Figures 2(a), for momentum flux, and 2(b), for buoyancy flux, show that this predicted behavior is observed in the presently computed results. Note that the quantity F in the figure represents

$$F = 2\pi \int_0^{R_o} \alpha g(W\Delta T + < wt >) r dr, \tag{12}$$

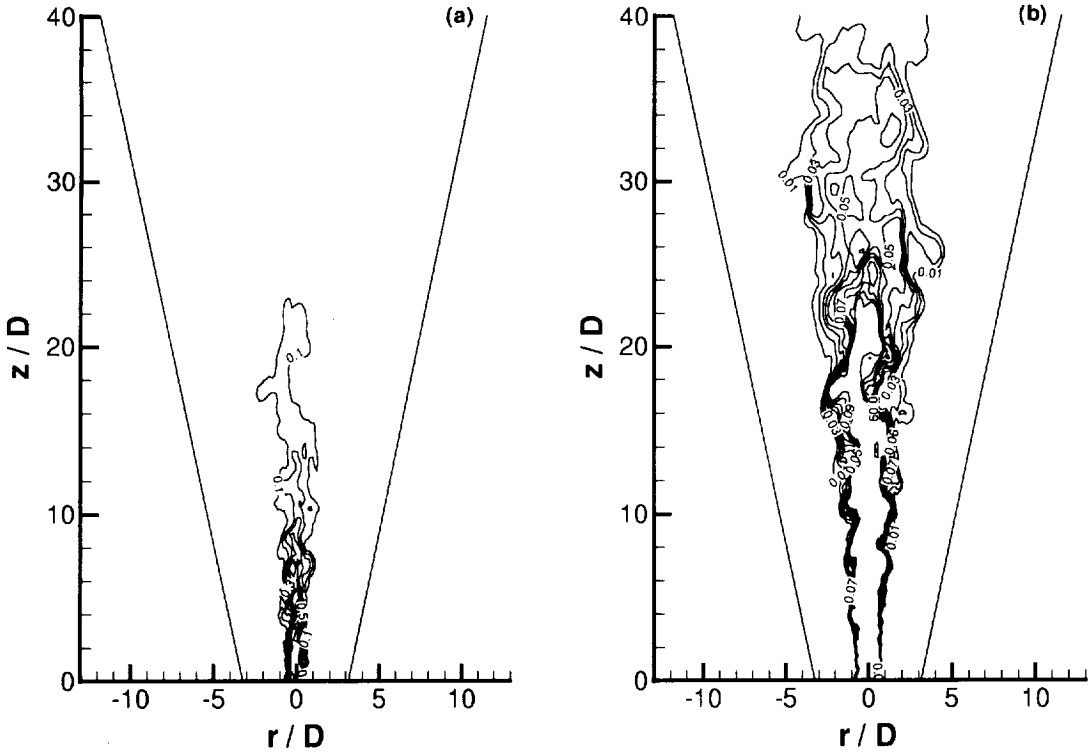

FIGURE 1. Distribution of computed temperature difference Θ in the buoyant plume at a non-dimensional time of 150: (a) contour levels from 0.1 to 1 in steps of 0.1, (b) contour levels from 0.01 to 0.1 in steps of 0.01. The computational domain boundaries along the lateral direction are also shown.

where $< wt >$ represents the turbulent contribution to the total buoyancy flux, w and t being the fluctuations in the streamwise velocity and temperature respectively.

The buoyancy flux shows a fall of about 15% in its value (with respect to that at the source) over the first 5 diameters as we go downstream from the source but remains quite constant afterwards. This indicates that the present computation quite faithfully represents the integral behavior of a buoyant plume in the self-similar region downstream, where the Boussinesq approximation is valid. The order of change in F over z predicted here is similar to that reported in the various experiments.

2.4.3 Mean flow

The results for streamwise variation of centerline mean velocity W_c and temperature difference ΔT_c are shown using the usual non-dimensional form (see, e.g., Shabbir & George 1994) in Fig. 3 using a log-log plot. As can be seen very clearly, the temperature distribution takes longer to achieve self-similarity when compared to the streamwise velocity; thus W_c achieves self-similarity around $z/L_M = 6$, whereas

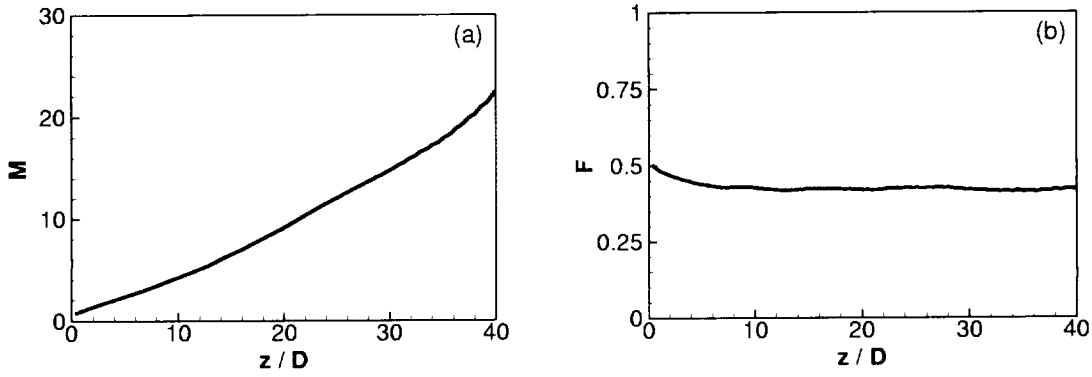

FIGURE 2. Streamwise variation of radially and azimuthally integrated (a) momentum and (b) buoyancy fluxes.

ΔT_c does so by $z/L_M = 15$. The scatter in the various reported experimental data is quite large, and the present results fall towards the high end of this scatter. The computed streamwise growth rates, however, are remarkably consistent with that predicted by the theory and experiments.

Next we look at the mean radial profiles of $< W >$ and $< \Delta T >$ at some streamwise stations in order to establish the self-similarity of the present computed results. Figure 4 shows the computed results along with Gaussian fits of available experimental data as compiled by Shabbir & George. The computed velocity profile closely matches that given by Rouse *et al.* (1952), is similar in width compared to the ones in Papanicolaou & List (1988), but is different from those reported by Shabbir & George (1994) and Nakagome & Hirata (1977) both in terms of the width of the profile and the maximum value at the centerline.

The computed temperature profiles differ from all the experimental ones in that the present ones are narrower. The centerline values, however, are close to that reported by Papanicolaou & List.

2.4.4 Turbulence properties

In Fig. 5, we present the computed results for the second order moments of fluctuating quantities using solid curves, along with the experimental data from Shabbir & George (1994) using symbols. The radial profiles of turbulence stresses at different streamwise stations converge quite well in the time over which they are averaged and show reasonable collapse when plotted using similarity variables. The present results for $< w^2 >$ and $< uw >$ are comparable to those obtained by Shabbir & George except for the width of the profiles. For the fluctuating stresses involving temperature, however, it is the magnitude which shows large differences, consistent with similar relative differences seen for radial mean profiles in Fig. 4 above. However, a few words of caution are in order: such comparisons between filtered stresses (as in the present case) with experimental results may not be very meaningful unless it can be shown that the subgrid stresses are small in comparison.

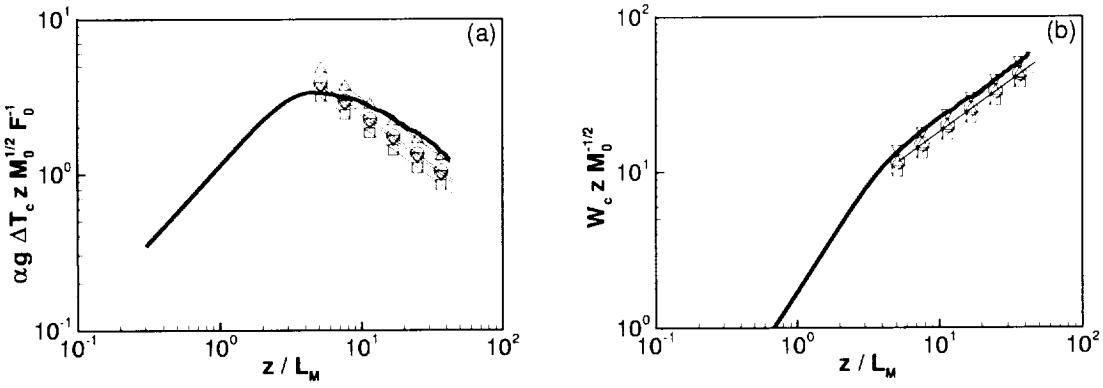

FIGURE 3. Normalized mean (a) buoyancy and (b) vertical velocity along the plume centerline plotted against the normalized distance z/L_M from the source. The bold lines represent the present computation. Fits to various experimental results are shown using lines with symbols (□ : Shabbir & George 1994, △ : Papanicolaou & List 1988, ▽ : Rouse *et al.* 1952, ○ : Nakagome & Hirata 1977).

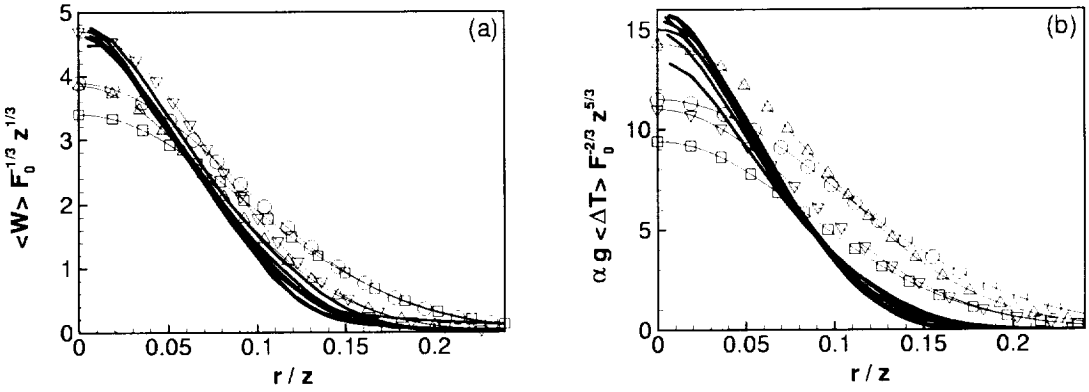

FIGURE 4. Radial profiles of (a) mean streamwise velocity and (b) mean temperature difference plotted in similarity form. The computed results at $z/D = 15$ to 40 at interval of 5 are shown using bold lines. The lines with symbols represent the experimental data as described in Fig. 3.

3. Conclusions and future plans

In the present preliminary study, we have shown that reasonable predictions of the evolution of a turbulent round buoyant plume can be obtained by means of LES with the dynamic subgrid model. The large scatter between available experimental data makes definitive comparison difficult. However, the present results fall within the scatter region of the experimental data.

Judging from the scatter in various experimental results, the boundary conditions are likely to play a significant role in this flow. The present computations also bring up various issues regarding the imposed conditions along the lateral and

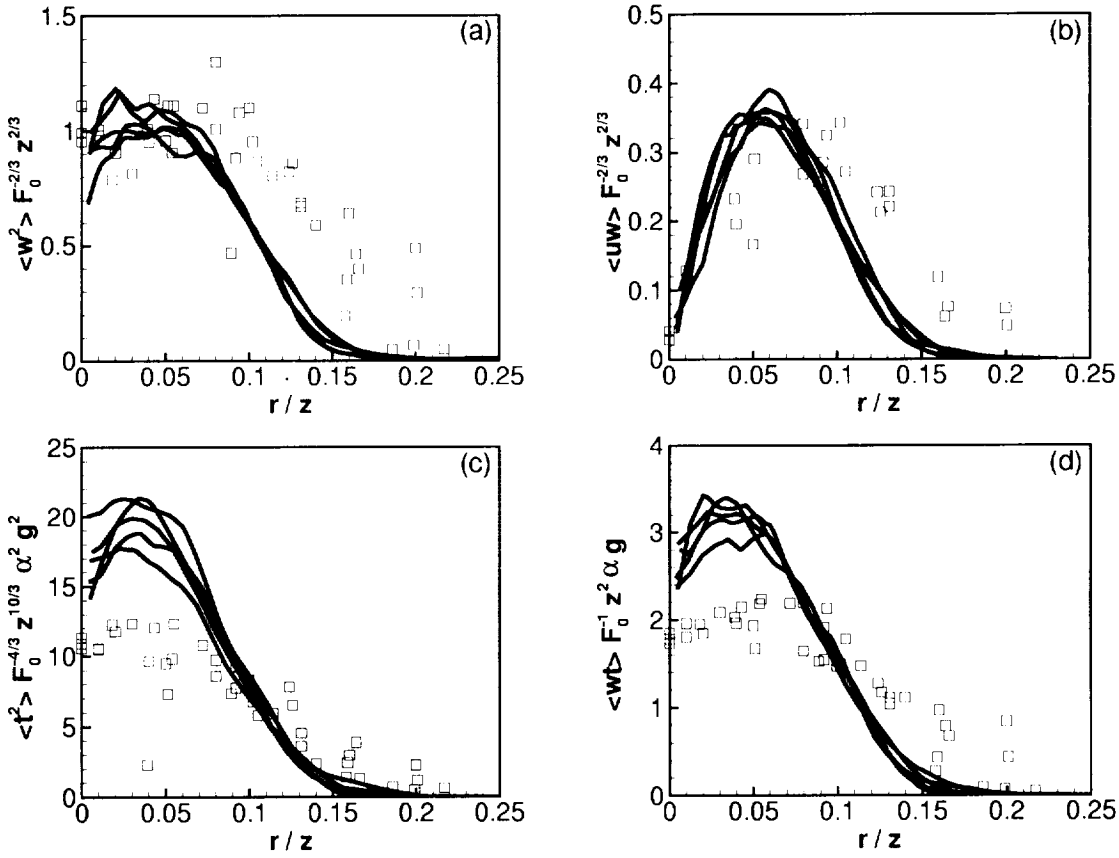

FIGURE 5. Second order moments plotted in terms of similarity variables. (a) the vertical velocity fluctuations, (b) the turbulent shear stress, (c) temperature fluctuations, (d) the vertical turbulent heat flux. The lines represent the computed results at $z/D = 20, 25, 30, 35$ and 40: the experimental data from Shabbir & George (1994) are shown superposed using □ symbols.

outflow boundaries. The traction-free condition along the lateral boundary can influence entrainment, and so can the advective condition and buffer zone along the outflow boundary. What should be the nature of the physically correct boundary conditions along such boundaries still remains an open question (see Gresho 1991 in this regard). We plan to probe further into this aspect, and study the effect of different boundary conditions. The effect of grid resolution and position of lateral boundaries will also be investigated.

Long term plans include LES of plumes in stratified environments and inclusion of cloud models in such flows.

Acknowledgments

The authors wish to thank Dr. Bendiks J. Boersma for making available his jet code, which has been modified for the present computations.

REFERENCES

BASU, A. J. & NARASIMHA, R. 1999 Direct numerical simulation of turbulent flows with cloud-like off-source heating. *J. Fluid Mech.* **385,** 199-228.

BATCHELOR, G. K. 1954 Heat convection and buoyancy effects on fluids. *Q. J. R. Met. Soc.* **80,** 339-358.

BOERSMA, B. J., BRETHOUWER, G. & NIEUWSTADT, F. T. M. 1998 A numerical investigation on the effect of the inflow conditions on the self-similar region of a round jet. *Phys. Fluids.* **10,** 899-909.

GERMANO, M., PIOMELLI, U., MOIN, P. & CABOT, W. H. 1991 A dynamic subgrid-scale eddy viscosity model. *Phys. Fluids A.* **3,** 1760-1765.

GRESHO, P. M. 1991 Incompressible fluid dynamics: some fundamental formulation issues. *Ann. Rev. Fluid Mech.* **23,** 413-454.

LILLY, D. K. 1992 A proposed modification of the Germano subgrid-scale closure method. *Phys. Fluids A.* **4,** 633-635.

LIST, E. J. 1982 Turbulent jets and plumes. *Ann. Rev. Fluid Mech.* **114,** 189-212.

NAKAGOME, H. & HIRATA, M. 1977 The structure of turbulent diffusion in an axisymmetrical thermal plume. *Proceedings 1976 ICHMT Seminar on Turbulent Buoyant Convection.* **361-372.**

PAPANICOLAOU, P. N. & LIST, E. J. 1988 Investigation of round vertical turbulent buoyant jets. *J. Fluid Mech.* **195,** 341-391.

PAPANTONIOU, D. & LIST, E. J. 1989 Large scale structure in the far field of buoyant jets. *J. Fluid Mech.* **209,** 151-190.

RODI, W. 1986 Vertical turbulent buoyant jets: experimental findings and prediction methods. *Proc. Intl. Symp. on Buoyant Flows*, Athens, Greece, Sept 1-5.

ROUSE, J., YIH, C. S. & HUMPHREY, H. W. 1952 Gravitational convection from a boundary source. *Tellus.* **4,** 201.

SHABBIR, A. & GEORGE, W. 1994 Experiments on a turbulent buoyant plume. *J. Fluid Mech.* **275,** 1-32.

VREUGDENHILL, C. B. & KOREN, B. 1993 Numerical methods for advection-diffusion problems. *Notes on Num. Fluid Mech.* **45,** Vieweg, Braunschweig.

ZELDOVICH, Y. B. 1937 Limiting laws for turbulent flows in free convection. *Zh. Eksp. Theoret. Fiz.* **7,** 1463.